VORTICAL FLOW OVER A 3-D BACKWARD-FACING STEP

T. P. Chiang and Tony W. H. Sheu
Department of Naval Architecture and Ocean Engineering, National Taiwan University, 73 Chou-Shan Road, Taipei, Taiwan, Republic of China

Numerical simulations of Navier-Stokes equations were performed for incompressible Navier-Stokes flow inside a channel. The flow field under investigation was characterized as having a backward-facing step, with an expansion ratio $\gamma = H / h = 1.9423$, over which a fully developed channel flow is suddenly expanded into the channel with a channel width, B, to upstream channel height, h, ratio $B / h = 2, 4, 6$, and 10. Numerical solutions for this backward-facing step problem were obtained on the basis of span ratios and Reynolds numbers. For the Reynolds numbers considered, $Re = 100, 389, 800$, we elaborate on the changes in the flow topology according to solutions computed at $Re = 389$. We use topology theory as a guide to studying flows that are kinematically possible. This theory is mathematically rigorous and helps find critical points, from which we can sketch complicated flow patterns by clarifying the three-dimensional flow separation just behind the step and the flow reattachment on the downstream roof. Clearly visible on the roof of the channel is the separation-reattachment flow feature. Notably addressed is that separated flow on the roof is only confined to regions near the two side walls and does not extend over the whole span. The onset of a near-wall pair of counterrotating vortices is associated with the presence of closed separation-reattachment bubbles. They are visible at transverse planes, just upstream of termination of the roof recirculation bubble, near the two end walls.

INTRODUCTION

Fluid flows characterized as having flow separation adjacent to a solid boundary have applications in many areas. Examples are flows around buildings, around microelectronic circuit boards, and in heat exchangers and ducts for industrial use. Of this class of flows, the flow over a simple geometry such as a backward-facing step may consist of the separation and reattachment of the flow.

Expansion flows in straight channels with steps have been the focus of intensive study over the last few decades and have been the subject of an international workshop [1]. The reasons for the proliferation of research for this flow are due primarily to its physical as well as practical importance. Although this flow represents one of the simplest expansion flows, the physics involved are rather

Received 17 May 1996; accepted 19 August 1996.
This work was supported by the National Science Council of Taiwan under Grant no. NCHC85-04-004.
Address correspondence to Professor Tony W. H. Sheu, Department of Naval Architecture and Ocean Engineering, National Taiwan University, 73 Chou-Shan Road, Taipei, Taiwan, Republic of China. E-mail: sheu@indy.na.ntu.edu.tw

Numerical Heat Transfer, Part A, 31:167–192, 1997

1040–7782/97 $12.00 + .00

NOMENCLATURE

B	width of the channel	u_{mean}	inlet mean velocity
h	height of the upstream channel	x_m	coordinate along m direction
H	height of the downstream channel	x_0	length of the channel behind the step
N_x	number of grid points in the streamwise direction	x_1	reattachment length, as measured from the step, of the primary eddy
p	pressure	x_4	separation length, as measured from the step, of the roof eddy
Re	Reynolds number		
S	nondimensional step height ($\equiv \gamma - 1$)	x_5	reattachment length, as measured from the step, of the roof eddy
t	time	γ	expansion ratio ($\equiv H/h$)
u_i	velocity component along i direction	ν	kinematic viscosity

complex. For a flow into an expansion in the form of a step, the boundary layer separates at the step corner, forming a new free shear layer. Experimental evidence [2–5] reveals the formation of a series of recirculating vortices and flow reversals downstream of the step. This flow is followed by a downstream developing channel flow. These three-dimensional (3-D) separation eddies have a significant impact on hydrodynamics, shear stress distributions, and heat transfer rates. Broadening our understanding of flow evolution in a channel with a sudden expansion is thus fundamentally challenging and of practical importance in fluid mechanics. A more extensive analysis into the understanding of flow separation in a sudden expansion channel has been conducted experimentally by Armaly et al. [2] and Goldstein et al. [3]. We consider this problem also to be computationally important because of the availability of the experimental data [2—8] and the simplicity of the geometry. This problem, as a result, has long served as a prototype for validation studies of incompressible Navier-Stokes computational fluid dynamics (CFD) algorithms. Most of the work in recent decades has focused on the laminar and fully turbulent flow regime. More recently, attention has been paid to the onset of three-dimensionality and early transition to turbulence [9]. Numerical studies of expansion flows of the type considered in this article have been mostly two-dimensional (2-D) [1, 10]. Comparatively few have been dedicated to 3-D calculations [11–16], a task worthy of further research.

Although previous experimental work, together with comparatively few 3-D numerical studies, has provided a great deal of information about the backward-facing step flow, questions still remain unanswered regarding the broad pattern of the recirculating flow structure behind the step. The present work is directed toward exploring the flow physics in great detail behind the expansion step, aided by a topological map of the inferred 3-D solutions for each test case. Due to space considerations, only representative results for Re = 389 carried out at $B = 10$ are shown.

The remaining sections are organized as follows. Working equations and the problem specifications are given in the following section. We then provide a brief outline of the segregated type algorithm, which is designed to compute the originally coupled finite volume discretization equations iteratively. The justification for using this analysis code is presented to give one a better idea of what

solution quality this code can offer. This is followed by an introduction of the employed continuous vector field theory, which provides a clear picture of the vortical flow structure. We chose the streamlines as the target vector field to explore vortical flow structure in depth by appealing to the theory of topology. With the finite volume solutions obtained, a topological study on these detailed computed primitive velocity vectors will provide insight into the vortical flow structure.

WORKING EQUATIONS AND PROBLEM SPECIFICATIONS

We consider here Newtonian fluids governed by the Navier-Stokes equations of motion, in the absence of a body force and subject to the incompressibility constraint condition:

$$\frac{\partial u_i}{\partial t} + \frac{\partial}{\partial x_m}(u_m u_i) = -\frac{\partial p}{\partial x_i} + \frac{1}{\mathrm{Re}}\frac{\partial^2 u_i}{\partial x_m \partial x_m} \tag{1}$$

$$\frac{\partial u_i}{\partial x_i} = 0 \tag{2}$$

In the above dimensionless primitive-variable framework, we denote $u_i(x_i, t)$ as the velocity components ($i = 1, 3$) and p as the isotropic pressure. According to Armaly et al. [2], the Reynolds number is defined as $\mathrm{Re} = u_{\mathrm{mean}} 2h/\nu$, where ν is the kinematic viscosity. For this study, lengths are normalized by the height of the upstream channel, h, while velocities are normalized by the inlet mean velocity u_{mean}. The application of the laminar flow model has been experimentally justified for $\mathrm{Re} < 1200$ [2]. For Re investigated here, the laminar assumption is thus legitimate.

The rationale behind the chosen velocity-pressure formulation is that this setting accommodates closure boundary conditions. In accordance with White [17], we prescribe an analytic unidirectional velocity profile at the step of the channel. Across this step, there is a sudden change in the area of the flow passage. Kaiktsis et al. [9] have investigated the sensitivity of the solutions to channel lengths upstream and downstream of the step. According to their study, variations in the flow field are difficult to examine among cases where fully developed inlet profiles are imposed as long as $\mathrm{Re} > 200$. Referring to Figure 1, which depicts the working physical boundaries, no-slip boundary conditions for velocities u_i are specified everywhere except at two planes, namely, the physical inlet and the synthetic outlet. No pressure boundary condition is permitted; otherwise, the problem under consideration will be overdetermined. We consider here extrapolation boundary conditions at a synthetic plane. Depending on Re, synthetic planes should be truncated at different lengths downstream of the step. The effect of the truncated dimensionless length x_0 on the channel flow has been also investigated by Kaiktsis et al. [9]. The flow was found to be affected, in comparison with the computed solutions underlying $x_0 = 34$ and 60 for Re much lower than 700. Approximately a 2% difference in the value of the reattachment length was reported in cases when

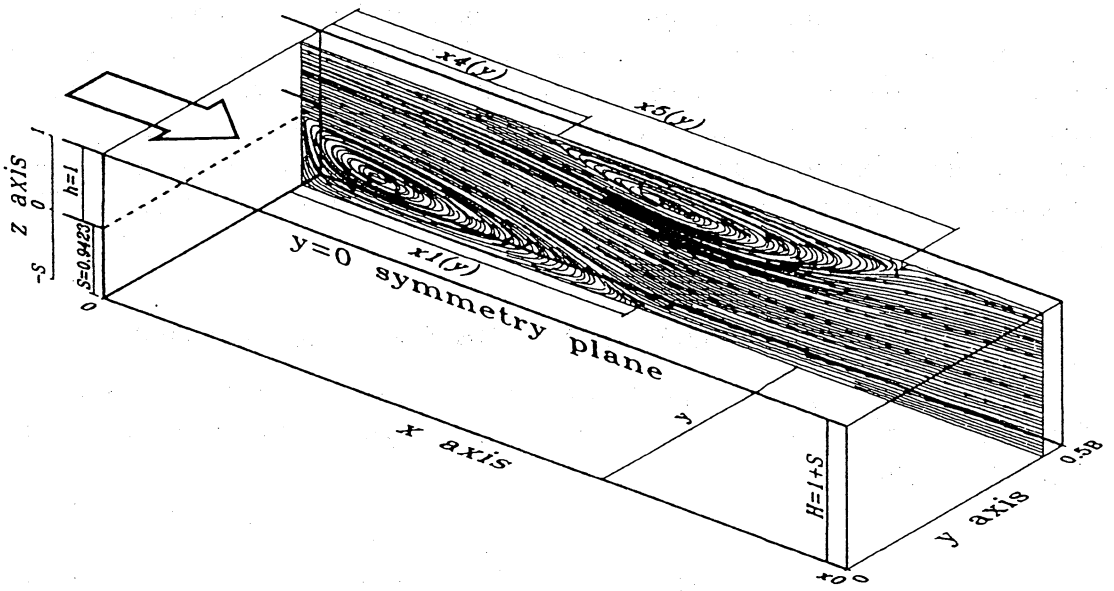

Figure 1. Geometry of 3-D channel with a backward-facing step.

Re $\geqslant$ 700. With this in mind, we consider $x_0 = 15, 35, 55$ for Re considered in this study, i.e., 100, 389, and 800. To mimic the physical experiment of Armaly et al. [2], further work is in progress to consider flow in a channel with a much larger width, namely, a channel width to upstream channel height ratio $B/h = 35$. An accurate numerical simulation for this laboratory experiment, however, far exceeds the computational resources available here. As a result, the spanwise lengths chosen for this study are 2, 4, 6, and 10.

FINITE VOLUME METHOD AND SOLUTION ALGORITHM

Having chosen working equations case in a primitive-variable form, we transform them into their algebraic counterparts so that they are amenable to computer simulation. To alleviate the well-known node-to-node pressure oscillations for problems defined at the incompressible limit, we advocate the use of staggered grids, although this grid setting adds considerable complexity to the programming. The choice of staggered grids follows the findings of Harlow and Welch [18]. The reasons for not using nonstaggered grids are twofold: first, a staggered grid obviates the need to devise appropriate interpolations [19–21] or to enforce an extra constraint compatibility condition [22], thus preventing pressure oscillations from occurring. Second, when faced with incompressible flow analysis, we lack the legitimate pressure boundary conditions for algorithms falling into the category of projection step methods. This difficulty has led to application of finite volume integration to a staggered grid setting with the control volume pertaining to continuity and scalar properties, and the other three to their respective momentum quantities. This amounts to saying that the pressure node is surrounded by three pairs of velocities (six degrees of freedom), which lie on the respective control surfaces.

Use of primitive variables will, furthermore, complicate the computation of incompressible Navier-Stokes equations owing to pressure unknowns. The absence of pressure in the continuity equation is the major cause of numerical difficulty, in that the already limited diagonal dominance of the indefinite nonsymmetric coefficient matrix is weakened further. Owing to ill conditioning, it is common to solve these linear algebraic equations using different variants of Gaussian elimination direct methods. Ill conditioning limits the choices of the algorithm designers for fully implicit formulations.

With knowledge, then, of this potential difficulty of mixed formulation, researchers were motivated to apply a segregated solution algorithm to incompressible Navier-Stokes flows. The rationale behind the algorithmic ideas of a segregated approach may be found in Ref. [23]. Instead of analyzing the working equations in a strongly coupled fashion, we derive a Poisson equation for the pressure difference as a means to compensate the pressure-velocity decoupling. This equation arises as a fractional-step equation and provides a mechanism for incorporating the incompressibility constraint through multiply staged equations. Such a pressure-correction algorithm complements the mixed formulation, in that it cuts down on the amount of overhead required to store the encountered matrix equations. Also, the semi-implicit scheme of SIMPLE [23], as applied to the present study, greatly enhanced stability and, in addition, provided the same steady state solution at less computational cost than the equivalent explicit scheme.

For flow at an angle to the grid line there is gross distortion of the advected profile. These false diffusion errors are particularly severe under high-Re circumstances. The streamline upwind discretization scheme is considered among the best methods to approximate nonlinear advective fluxes and is thus referred to. We apply here the QUICK scheme of Leonard [24] to a flow domain that has been nonuniformly discretized. Since discretization errors arising from curvilinear coordinate transformation are generally considerable and hard to resolve for configurations involving an abrupt change or for curvilinear lines having appreciable curvature, we employ a Cartesian coordinate system. We conclude this section by noting that the use of a streamline upwind advection scheme in Cartesian coordinates can produce a more accurate solution, so that the detailed flow physics can be rendered.

VERIFICATION OF COMPUTER CODE

Usually, a reliable computer simulation of an engineering problem is preceded by a series of numerical tests. These tests can be grouped into three classes of problems: verification, benchmarking, and validation. As a first step to investigating the accuracy of the algorithm and scheme implementations, it is important to provide a definite verification of the computational method. In this regard, we consider the analytic problem of Ethier and Steinman [25] in a cubic $\Omega(-1 \leqslant x, y, x \leqslant 1)$.

As is usually done, we assess here the employed QUICK-type upwind discretization scheme and semi-implicit solution algorithm on the basis of nodal values computed in the uniformly discretized domain. We then sum the prediction nodal errors in an L_2 norm sense. With continuous refinement of grid spacings, we

can compute the rate of convergence. According to the errors computed against grid spacings, the rates of convergence for velocities and pressure are 1.71 and 1.3, respectively. The reader is referred to Refs. [26, 27] for additional details. The code verification results for incompressible flow analysis provide us with sufficient confidence to proceed with the subsequent benchmarking and validation problems. The present study considers a 3-D expansion flow in a channel with a sudden step, with an emphasis on both Re and spans of the channel.

EXAMINATION OF A VORTICAL FLOW STRUCTURE: A TOPOLOGICAL STUDY

Rapid progress in computer technology has made 3-D computations less expensive and more feasible. This accompanies renewed interest in studying 3-D flow structures. Detailed study of a considerable body of data is an enormous task and is practically impossible using conventional methods. Researchers have resorted to new methodologies that permit more effective visualization of pertinent flow structures. There are a few approaches to achieving this goal in the literature. The following is an attempt to give a favor of the subject and provides a justification for the underlying principle of this subject area in many engineering disciplines. For a comprehensive introduction to these approaches, the reader is referred to Yates and Chapman [28].

Of the possible methodologies to explore the kinematics of complex flows, we have the choice of conducting a topological study of vector quantities such as streamlines [29] or skin-friction lines [30] or carrying out a graphic visualization of a scalar quantity, namely, density of helicity or normalized helicity [31]. We will concentrate on the topological study of limiting streamlines. The rationale for this choice is that the flow structure can be best described by the topological properties inferred from computed streamlines. Following Legendre [29], the study of the topology of 3-D streamlines projected onto a no-slip body surface is the computational analogy to the experimental surface flow visualization, bearing in mind that the skin-friction line field, according to the definition of Lighthill [30], can be regarded as the projection of the 3-D streamline field onto the body surface. This implies that the observed topological patterns of limiting streamlines have significant implications for the flow evolution in the vortical flow field.

The kinematic aspects of computable limiting streamlines are best described in terms of singular points. Determination of these singular points, from which the flow structure can be sketched, is thus of importance. In a set of velocity vectors, singular points are, by definition, classified as having zero magnitudes, and therefore their directions are indeterminant. Around a critical point, the vector field varies according to the eigenvectors and the eigenvalues of the Jacobian of the velocity field at the detected critical point. Depending on the divergence of the shear stress vector and the Jacobian just mentioned, the singular points can be classified into two main topological types: nodal and saddle points [28].

Saddle points are distinguished from nodes by their portraits. Passing through saddle points, there exist only two shear stress lines, on each of which the direction of the skin-friction vector field ($\mu(\partial u/\partial z)$, $\mu(\partial u/\partial z)$) changes sign on a surface z = const. Depending on the classification of saddle points, separation or attach-

ment, both skin-friction directions point toward the critical point on one, and both point away from this point on the other. This implies that saddle points act as barriers in the field of vectors. Nodal points, on the other hand, are classified as points through which pass an infinite number of shear-stress lines.

Nodal points fall into two groups, namely, regular nodal points (or nodes) and foci (or spiral nodes). Nodal points of attachment act as sources of skin-friction lines that emanate from the point and spread out over the surface. Nodal points of separation, on the other hand, act as sinks where the skin-friction lines circumscribing the body surface vanish. Foci and nodes differ in their orientation of the chosen vector field. For a singular point defined as a spiral node, all shear stress lines spiral onto or out of this point. Emanating from this class of nodes are two straight critical lines.

COMPUTED RESULTS

The present study has sought to elucidate the expansion flow structure behind the step. Among numerical difficulties that complicate most inflow-outflow simulations is ambiguity in determining the cutoff downstream plane. Improper specification of outflow boundary conditions will erroneously introduce unresolved nonphysical disturbances. Errors arising from the open boundary will further propagate upstream through boundary layers that are attached to the roof, floor, and two side walls of the channel. Unfortunately, the most appropriate outflow boundary conditions at the synthetic outlet are still far from well understood and need further study. Gaining a better understanding of this closure problem therefore has been the focus of many previous studies. Interested readers are referred to Ref. [32].

Here, there is no intention to apply a high-order downstream condition such as the mixed Neumann/viscous-sponge boundary condition [33] to eliminate spurious instabilities arising from an erroneous specification of outflow boundary conditions. To compensate for the potential loss of stability, we prescribe a very simple setting of outflow boundary conditions at a streamwise location that is sufficiently downstream of the step. These outflow conditions are characterized as having zero-velocity gradients. At the upstream inlet, we provide the unidirectional velocity profile, as given in Ref. [17], in a straight channel with a cross-sectional area $h \times B$. Numerical exercises reveal that this flow accommodates symmetry of the flow for the investigated Re. Exploiting this feature, only half of the channel is included in the model domain, subject to a set of symmetric boundary conditions at the spanwise plane $y = 0$. At the rest of the solid boundaries, the usual no-slip boundary conditions apply. Measurements done by Armaly [2] suggest that flows remain laminar for $\mathrm{Re} < 1200$. This experimentally verified laminar flow regime avoids complications of invoking turbulence modelings and thus simplifies the analysis.

Step corner and boundary layer development are among the considerations that are crucial to discretizing the physical domain of interest. For physical reasons, we cluster meshes near the two end walls, the step plane, the regions of separation, and the curved streamlines to resolve high-gradient velocity profiles. As shown in Figure 2, half of the channel is covered with mesh points $N_x \times 17 \times 40$ in the

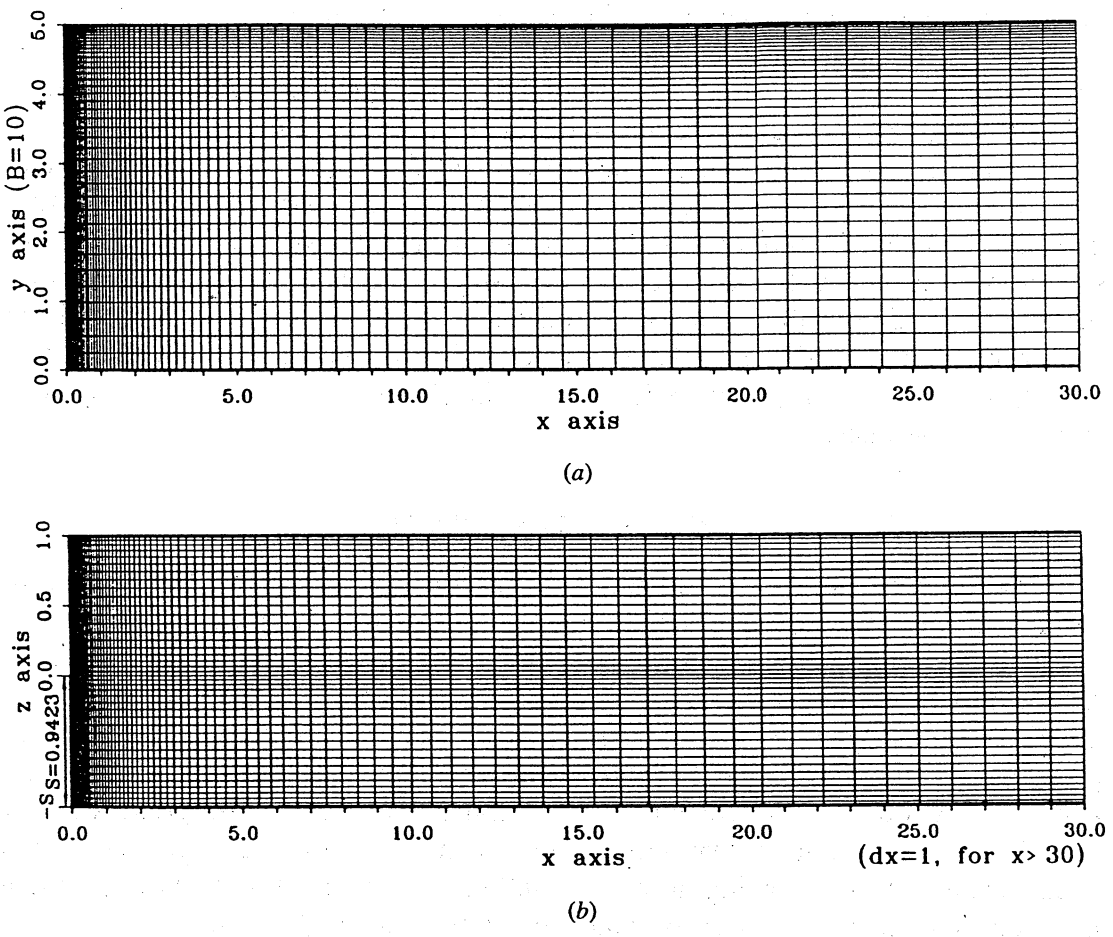

Figure 2. Clustered computational grid used for $B = 10$. (*a*) Grids on x–y plane; (*b*) grids on x–z plane.

narrow case of $B = 2$, while $N_x \times 37 \times 40$ in the wider case of $B = 10$. In our studies the values of N_x are 60, 80, and 100 for the chosen Re of 100, 389, and 800, respectively. Owing to space considerations, only the plots inferred from flow conditions given by Re = 389 and $B = 10$ are illustrated to show the complexity of the flow.

On the downstream roof, as shown in Figure 3, a separation-reattachment flow pattern has been found only within a limited extent, say, in the range of $0.4 < y/B < 0.5$. In contrast to 2-D solutions, where the roof separation-reattachment phenomenon becomes visible at Re = 450, as shown in Figure 4, a 3-D separation bubble on the roof near the symmetry plane is not detected in Figures 5–8 for any Re and spans considered, nor is flow reattachment detected. It is worth noting that the streamline patterns differ from those based on 2-D analysis. As Figure 9 indicates, the 2-D flow structure is characterized by a closed separation eddy. In the 3-D flows, closed streamlines, as shown in Figure 10, are visible only in regions near $y \sim 0.425B$. In the range of $0.425B \leqslant y \leqslant 0.5B$, the core flows tend to be drawn into the eddy, while the flows are drawn out of the eddy in the range of $0 \leqslant y \leqslant 0.425B$.

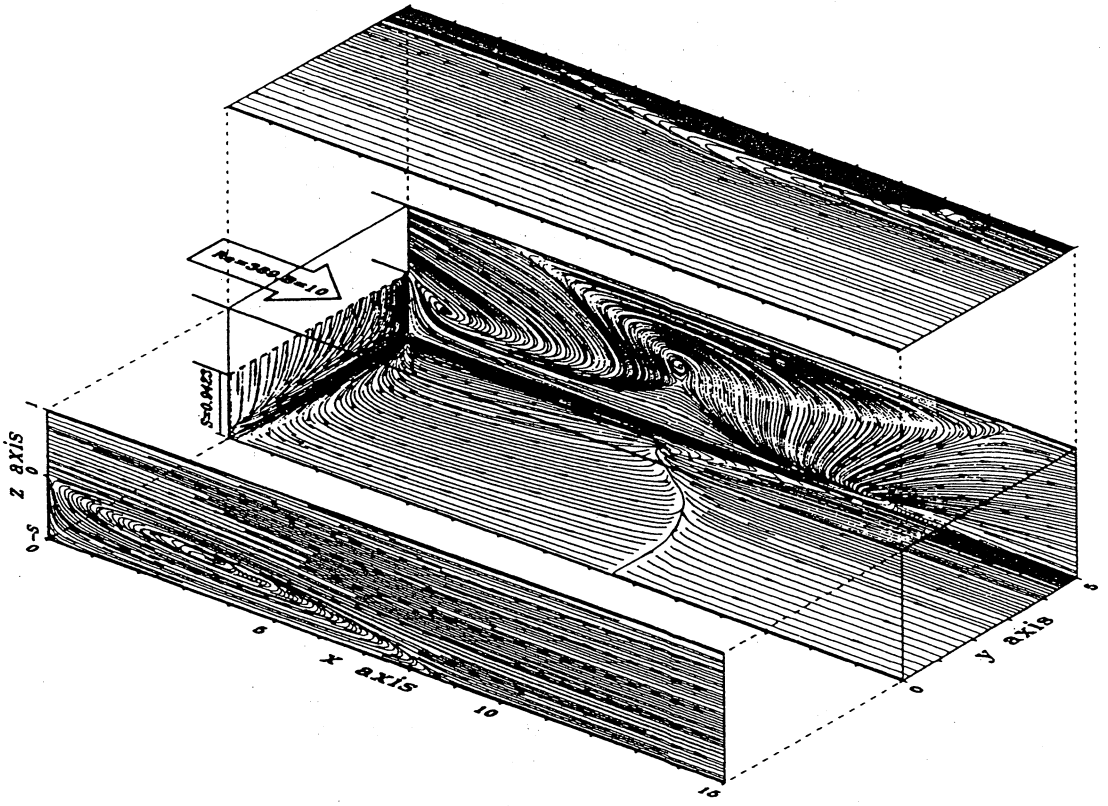

Figure 3. Perspective view of streamlines on the symmetry plane and limiting streamlines at roof, floor, and the vertical end wall for the case of Re = 389 and $B = 10$.

Among the basic features pertinent to the problem, as illustrated in Figure 1, is the flow separation from the step corner. As in many real flows, separation of a boundary layer is followed by downstream reattachment to a solid surface. Understanding the reattachment location, as measured form the step, is thus the important task of this study. Also of importance in the channel is the separation-reattachment eddy on the upper roof. These eddy sizes vary with Re considered. Rational characterization of the regions of circulation is thus greatly needed. To this end, determination of separation and attachment lines, and then the separation and attachment surfaces has been the focus of many previous studies. A topological study of the 3-D vector field and a flow visualization of helicity lend themselves to a precise mathematical formulation. We apply the theory of the topological of continuous vectors as the mathematical basis in finding singular points, from which the flow structure can be sketched. Given that skin-friction lines on a body surface are equivalent to limiting streamlines on a plane immediately adjacent to that surface, we plot limiting streamlines at planes immediately adjacent to the two end walls, and to the bottom as well as upper surfaces. Following Legendre's terminology [29], flow patterns thus obtained are considered as trajectories having properties consistent with those rendered by the experimental oil-streak lines. For brevity, we plot in Figure 3, limiting streamlines at $z = 0.9999$, -0.9423, $x = 0.0001$, and $y = 4.999$ for Re = 389 in the channel having the largest span. Clearly visible in Figure 3 are singular points, classified

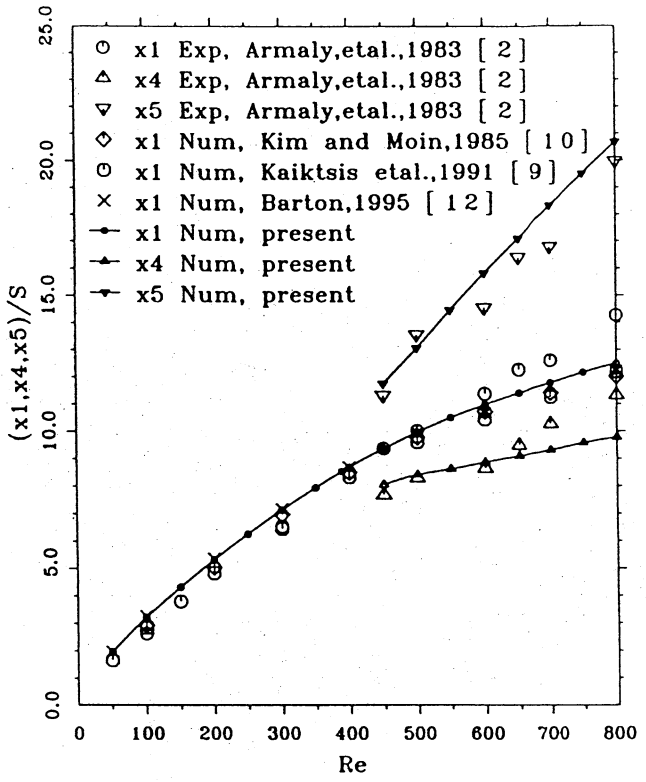

Figure 4. Comparison study on the computed 2-D reattachment lengths x_1 and x_5 and the separation length x_4.

specifically as the saddle points, on a plane adjacent to the end wall. According to the direction of these streamlines, separation and attachment lines are clearly identified and are regarded as barriers.

The line of separation is specific, in that for lines of this class, neighboring streamlines converge to it. However, from either side of a line of attachment, streamlines tend to diverge. According to this definition, the flow reattaches on the floor, while both flow separation and attachment are visible on the roof of the expansion channel. On the roof the presence of a circulating eddy near the end wall is the consequence of an adverse pressure gradient caused by the sudden expansion at the step edge. The flow recovers downstream and reattaches to the upper wall, followed by a gradual flow development into a fully-developed profile along the downstream direction. For clarity, we plot separation and reattachment lines against the spanwise locations in Figures 11 and 12 for several investigated Re.

Examination of a 3-D flow field can be carried out in many ways. Figures 13–15 plot streamwise velocity profiles at the symmetry plane against x, starting from the step and continuously extending to the truncated outlet. On increasing the width of the channel, velocity profiles progressively converge onto profiles computed on the basis of 2-D analysis, as shown in Figures 13*a*, 14*a*, and the

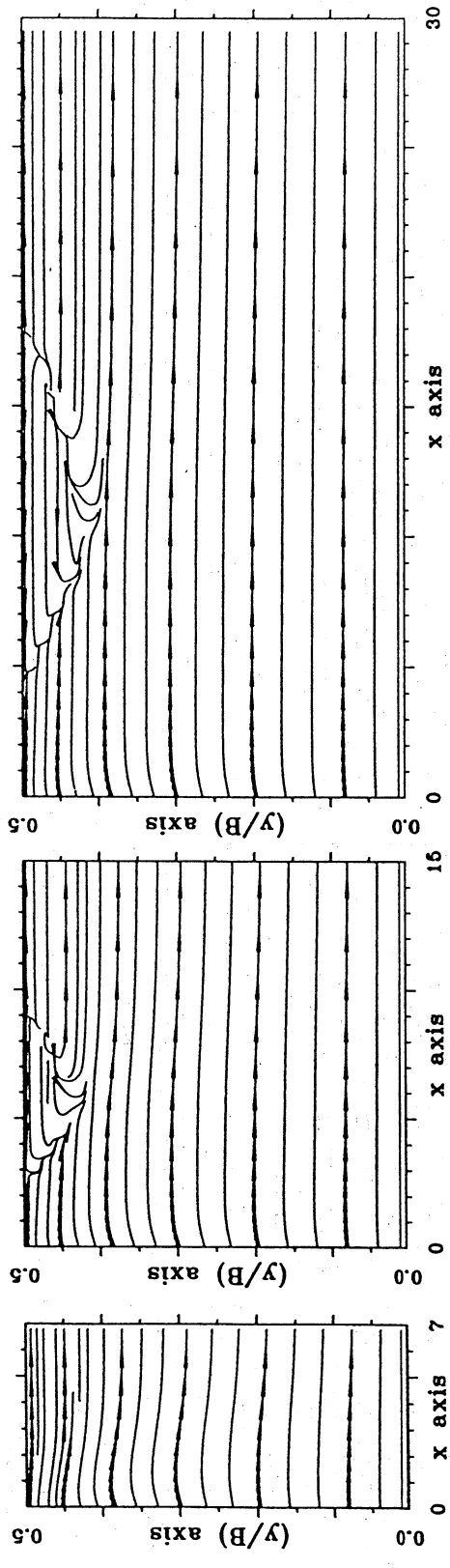

Figure 5. Computed limiting streamlines on the roof of the channel for the investigated span $B = 2$. (*a*) Re = 100, (*b*) Re = 389, and (*c*) Re = 800.

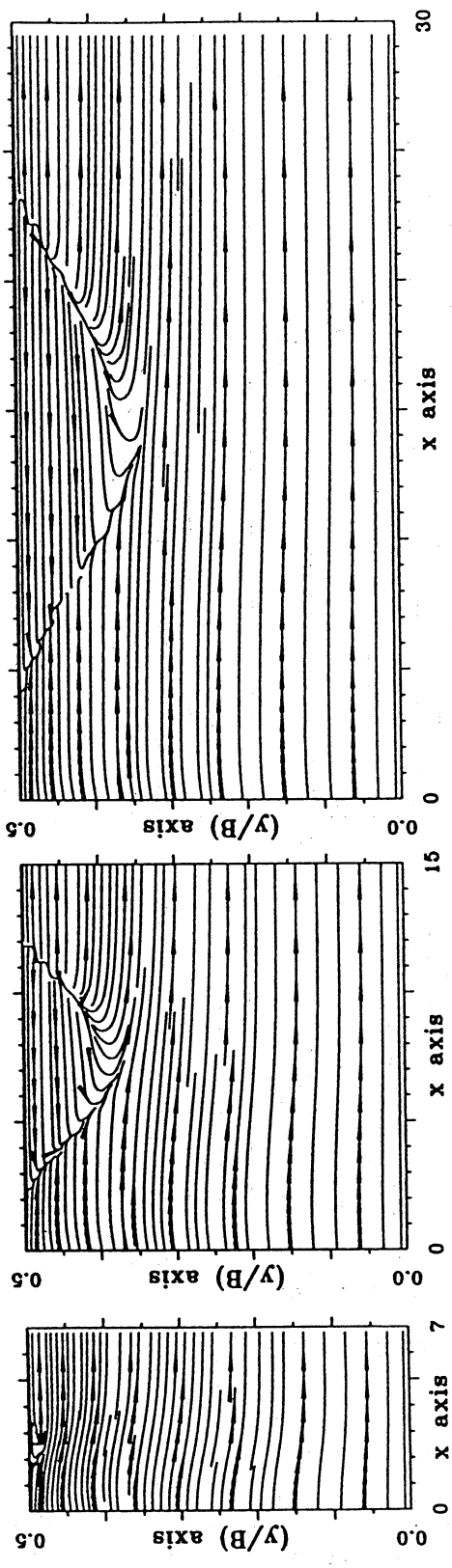

Figure 6. Computed limiting streamlines on the roof of the channel for the investigated span $B = 4$. (*a*) Re = 100, (*b*) Re = 389, and (*c*) Re = 800.

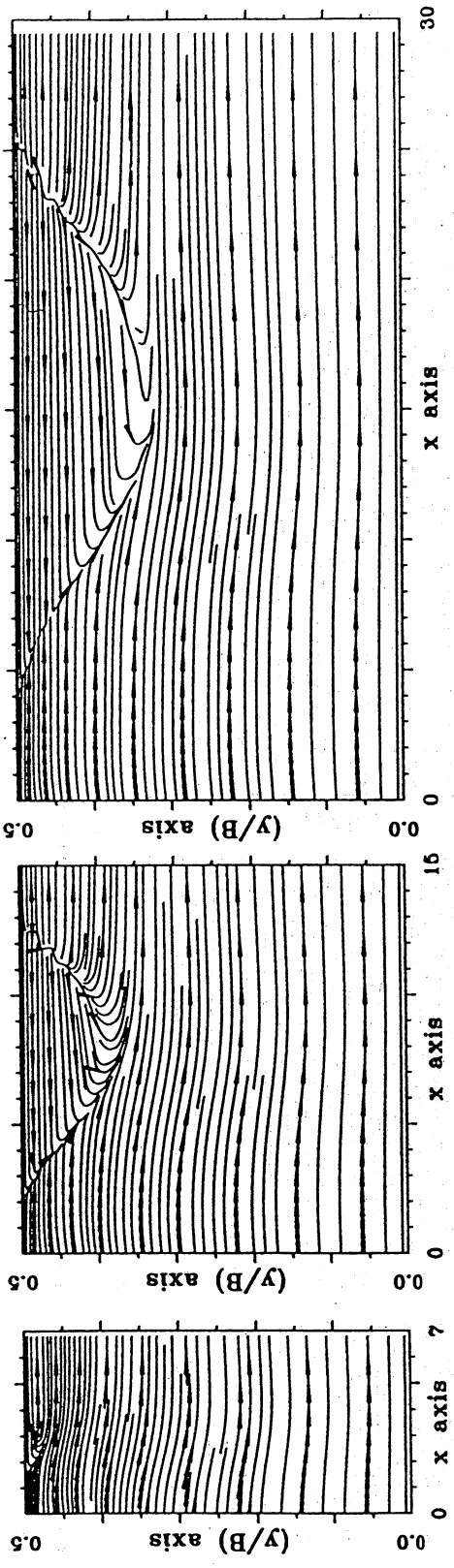

Figure 7. Computed limiting streamlines on the roof of the channel for the investigated span $B = 6$. (*a*) Re = 100, (*b*) Re = 389, and (*c*) Re = 800.

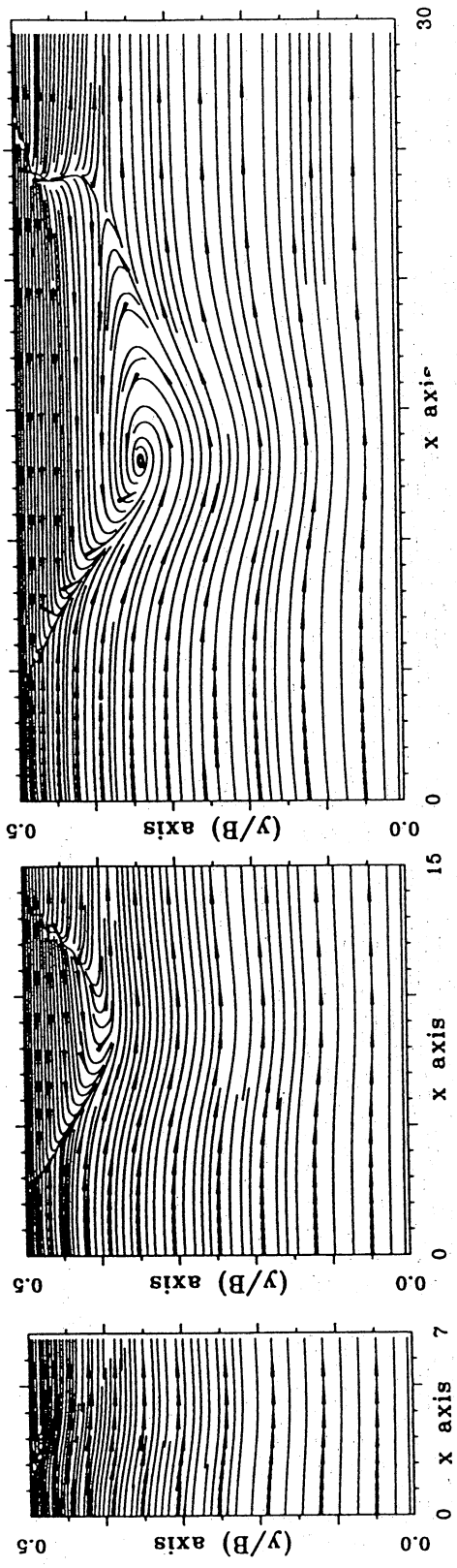

Figure 8. Computed limiting streamlines on the roof of the channel for the investigated span $B = 10$. (*a*) Re = 100, (*b*) Re = 389, and (*c*) Re = 800.

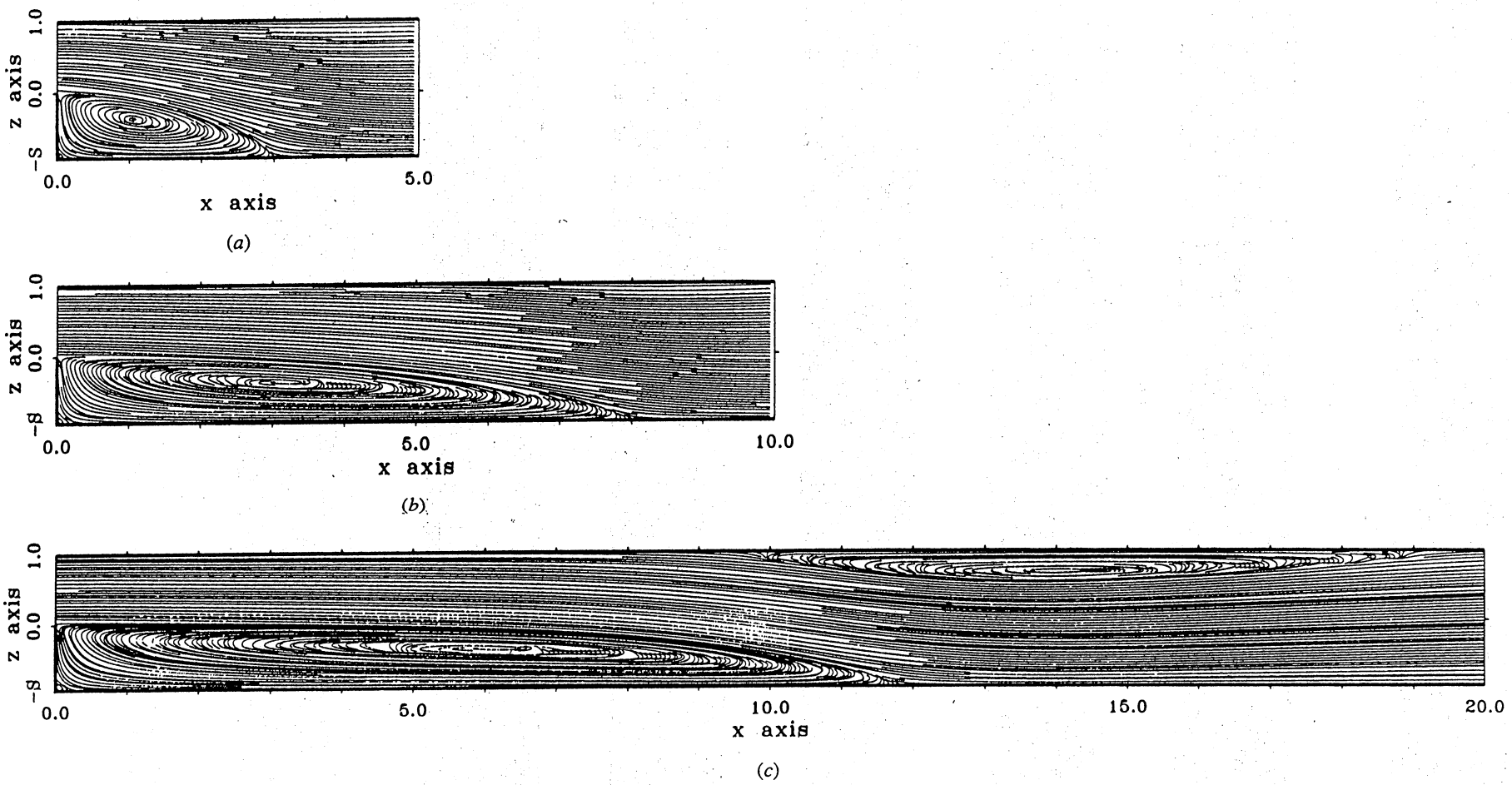

Figure 9. Computed streamlines based on the 2-D model for different Reynolds numbers. (*a*) Re = 100, (*b*) Re = 389, and (*c*) Re = 800.

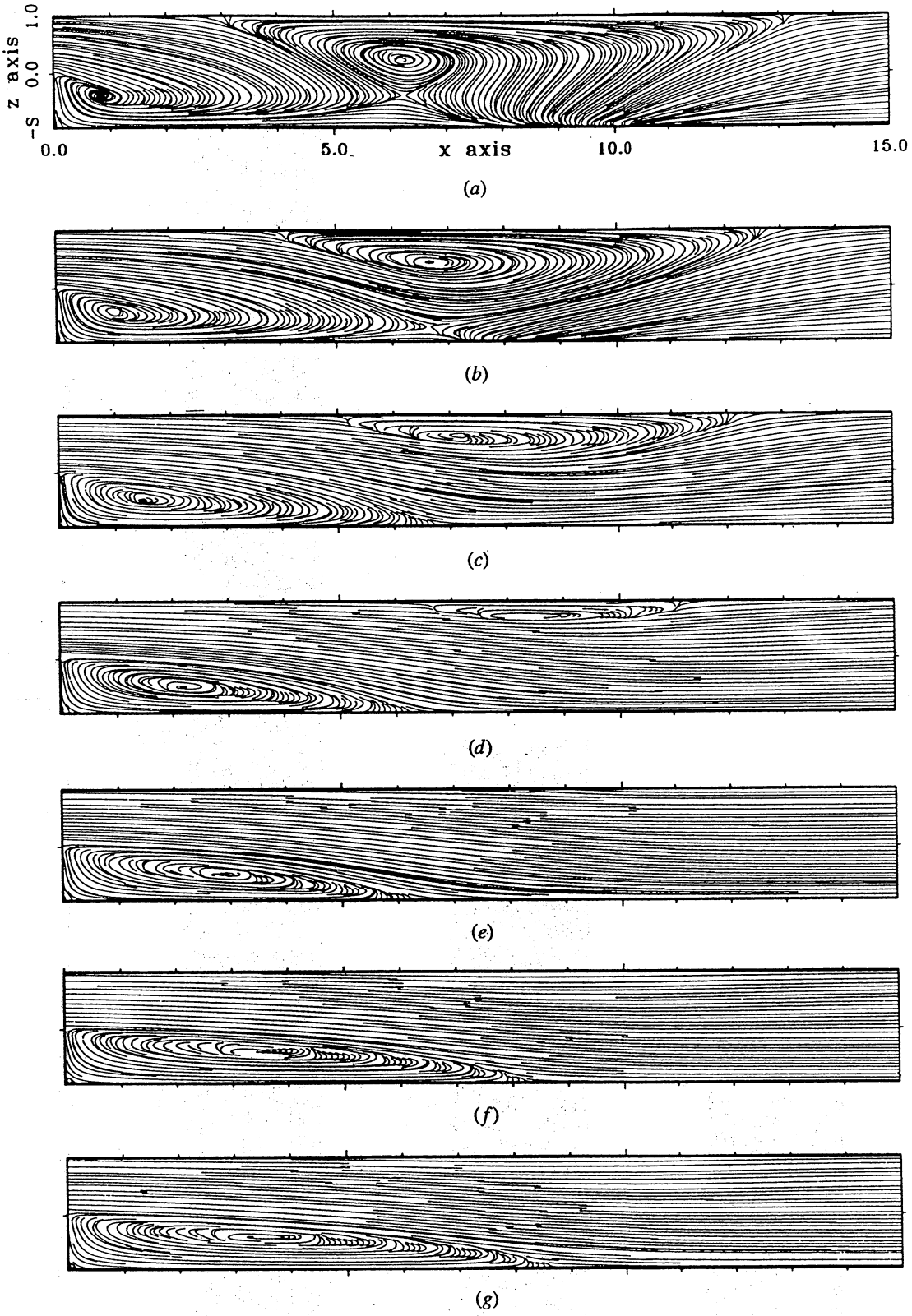

Figure 10. Computed streamlines at different planes for the case of Re = 389 and $B = 10$: (*a*) $y = 0.49B$, (*b*) $y = 0.47B$. (*c*) $y = 0.45B$, (*d*) $y = 0.425B$, (*e*) $y = 0.4B$, (*f*) $y = 0.2B$, and (*g*) $y = 0B$.

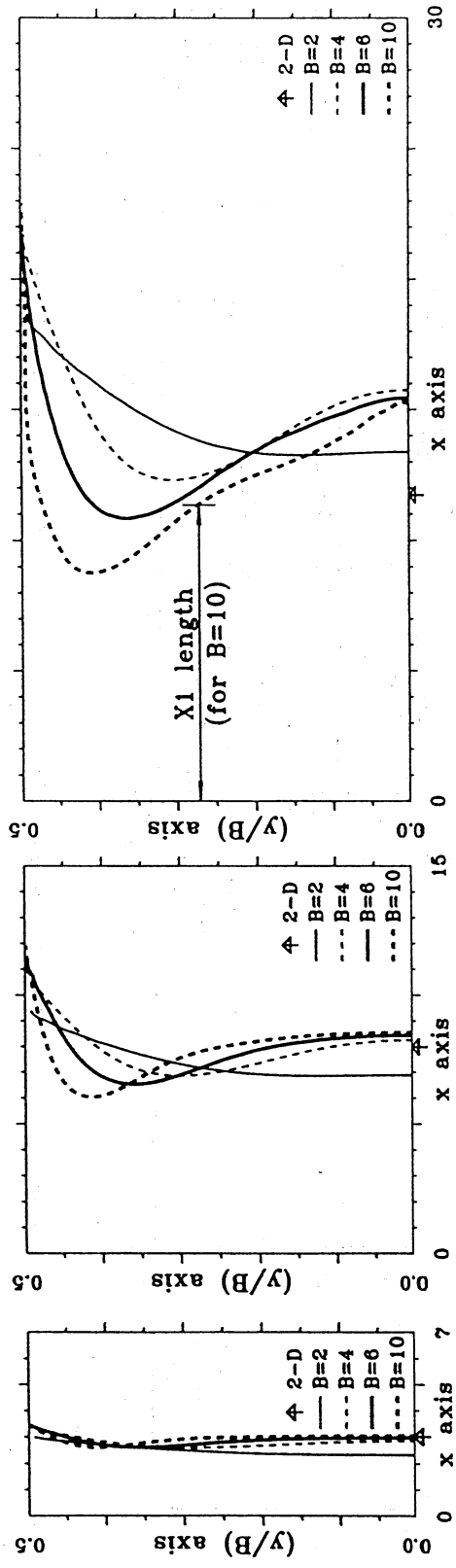

Figure 11. Change of reattachment length x_1 versus y for different Reynolds numbers. (*a*) Re = 100, (*b*) Re = 389, and (*c*) Re = 800.

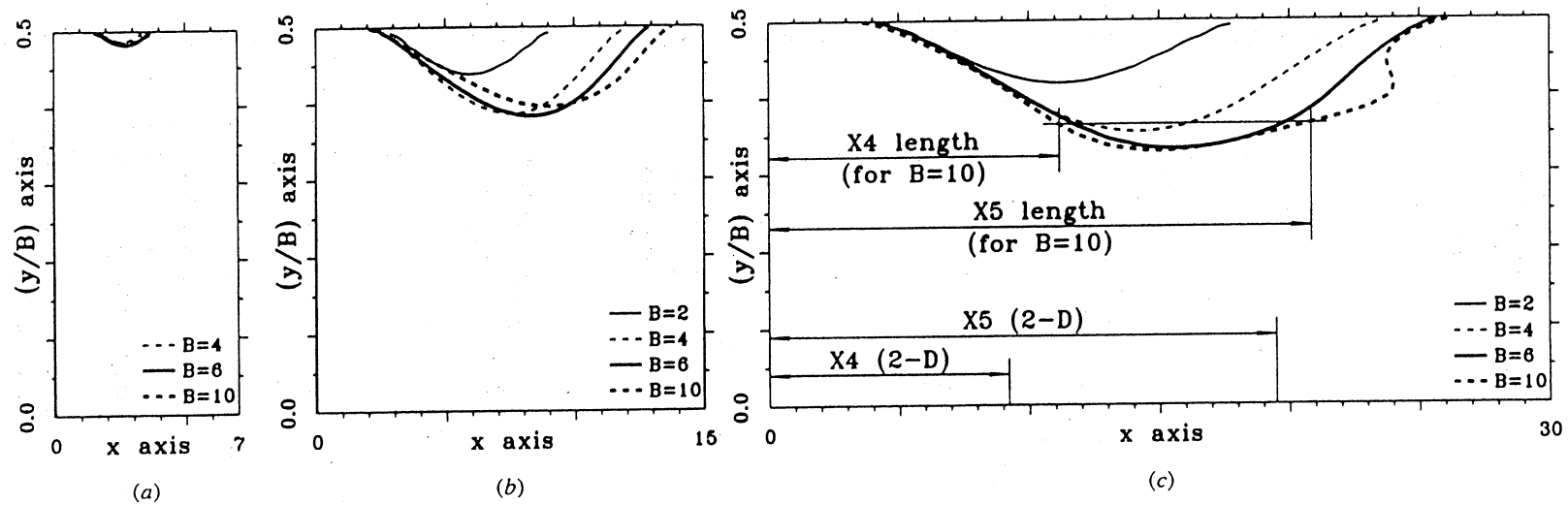

Figure 12. Change of separation length x_4 and reattachment length x_5 versus y for different Reynolds numbers. (*a*) Re = 100, (*b*) Re = 389, and (*c*) Re = 800.

experimental data of Armaly et al. [2] except in regions roughly between x_4 and x_5. This finding suggests the influence of the width of the channel on the downstream flow development. For the sake of comparison, we also summarize in Figure 4 the numerical results of 2-D calculations done by several investigators; also included are the experimental data of Armaly et al. [2] for the same step geometry with expansion ratio $\gamma = 1.9423$. Irrespective of the numerical approach followed, there exists consistent underestimation of the recirculation length x_1 above Re $\approx$ 600. Indeed, above a characteristic Re, the bifurcation of the steady, 2-D laminar flow into a 3-D flow is likely to be the primary source of discrepancies between the 2-D numerical solutions and experimental data.

Another effective means of elucidating a complex 3-D flow structure is to trace particles. Figure 16 shows 3-D traces of particles released downstream, one near the end wall at $y/B = 0.49$, one near the symmetry plane at $y/B = 0.01$, and the rest at $y/B = 0.37$, 0.25, 0.13. These points are all located away from the bottom wall with a height of $z = 0.1$. Viewed from the span direction, a particle tracer seeded near the end wall spirals along the span direction in an increasingly larger loop. As the symmetry plane is approached, the spiraling particle is lifted up, followed by a nearly 2-D plane motion. For the rest of the particle release points, the particle tracks reveal a simple 2-D pattern. In the course of spanwise spiraling flow motion, sign switching of velocity v is observed only in a few regions, which are limited to finite small spans.

We conclude this article by plotting streamlines in Figure 17, from which the onset of a pair of counter rotating vortices is closely associated with the separation-reattachment bubble at the roof of the channel. Indicative of the flow reversals and the downstream developing channel flow are the pressure contours plotted on the surfaces given in Figure 18.

CONCLUSIONS

This article has presented some fundamental flow structures pertinent to the 3-D backward-facing step problem. The numerical method employed here has been analytically verified with emphasis on the rate of convergence. Particularly important in studying 3-D kinematically possible flows is adoption of a method capable of providing a framework of considerable theoretical foundation. By appealing to the topological theory, we have been able to sketch the flow structure by finding singular points from the computed limiting streamlines. This topological study reveals the surface flow topologies, which are the experimental analogy to the oil-streak lines, by the presence of separation and attachment critical points. With the aid of the theory of topology of continuous vector fields, we can identify saddle points inside the channel. This finding has important implications in the interpretation of flow unsteadiness, which is due naturally to the formation of a global line of separation. Also, the separation line on the bottom wall and the separation proceeding continuously with the attachment line on the upper wall of the channel can be precisely determined. To extend our understanding of the flow physics inside a channel having a backward-facing step, we have performed a parametric

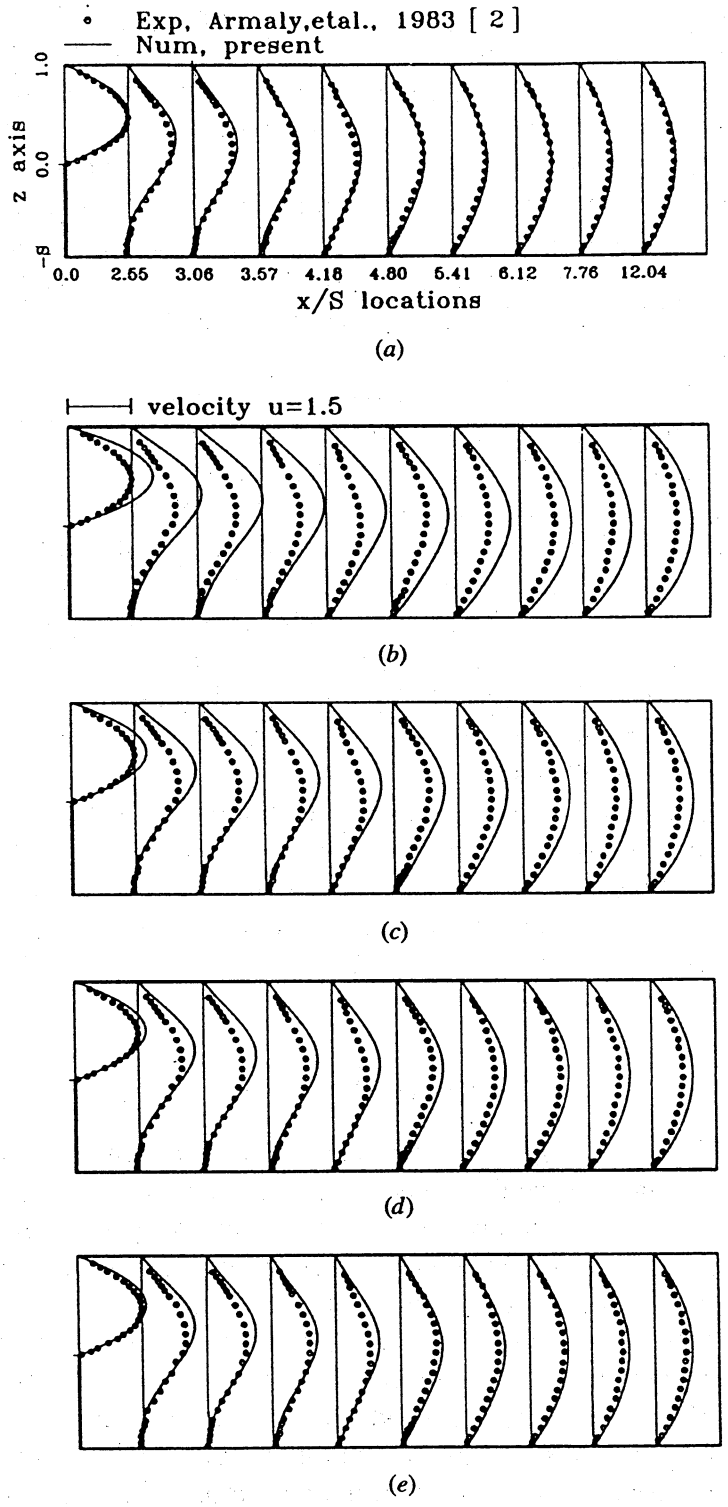

Figure 13. Comparison of computed velocity profiles (solid lines) with those of Armaly (open circles) at the symmetry plane for the case of Re = 100: (*a*) 2-D data, (*b*) 3-D with $B = 2$, (*c*) 3-D with $B = 4$, (*d*) 3-D with $B = 6$, and (*e*) 3-D with $B = 10$.

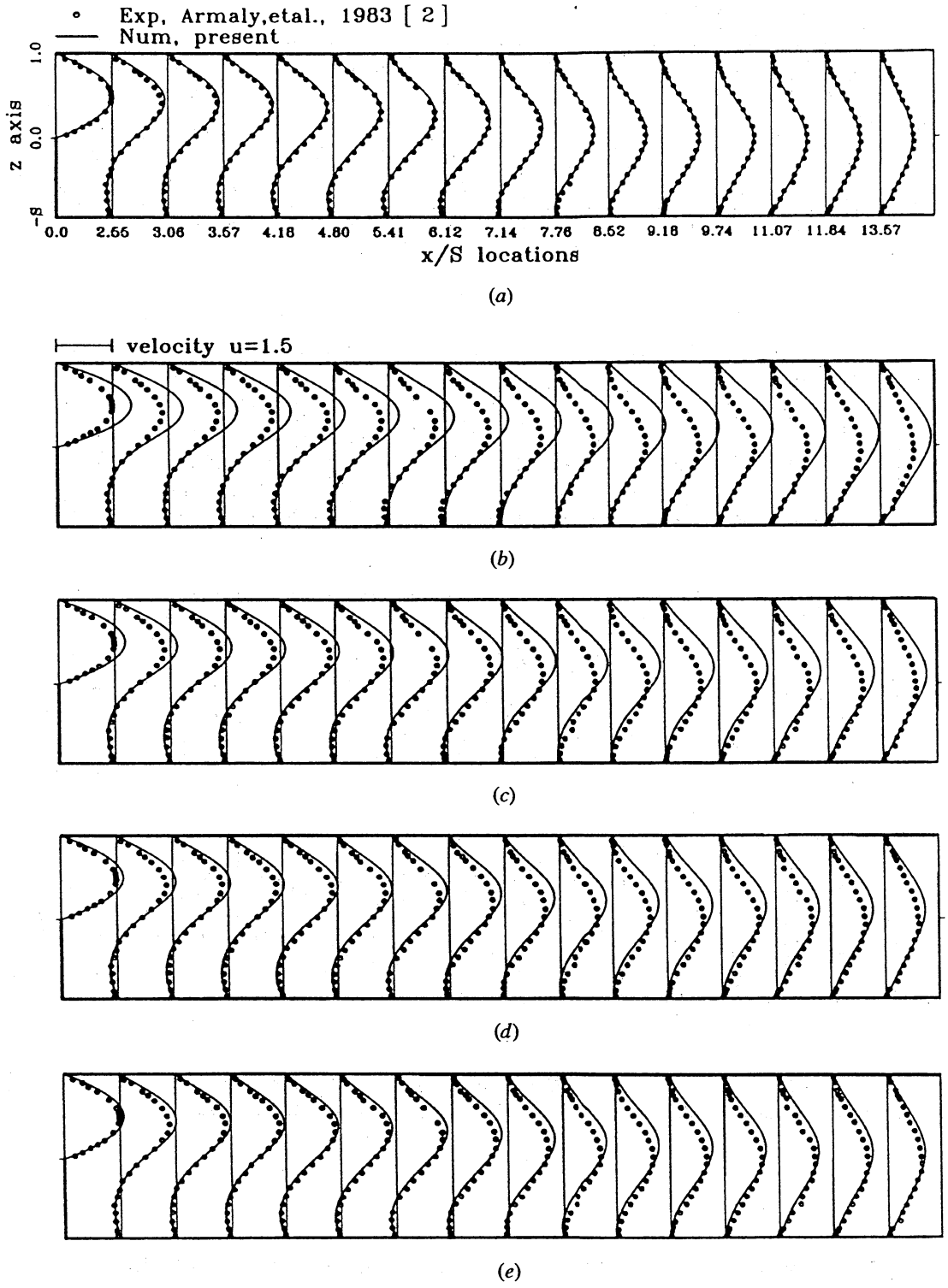

Figure 14. Comparison of computed velocity profiles (solid lines) with those of Armaly (open circles) at the symmetry plane for the case of Re = 389: (*a*) 2-D data, (*b*) 3-D with $B = 2$, (*c*) 3-D with $B = 4$, (*d*) 3-D with $B = 6$, and (*e*) 3-D with $B = 10$.

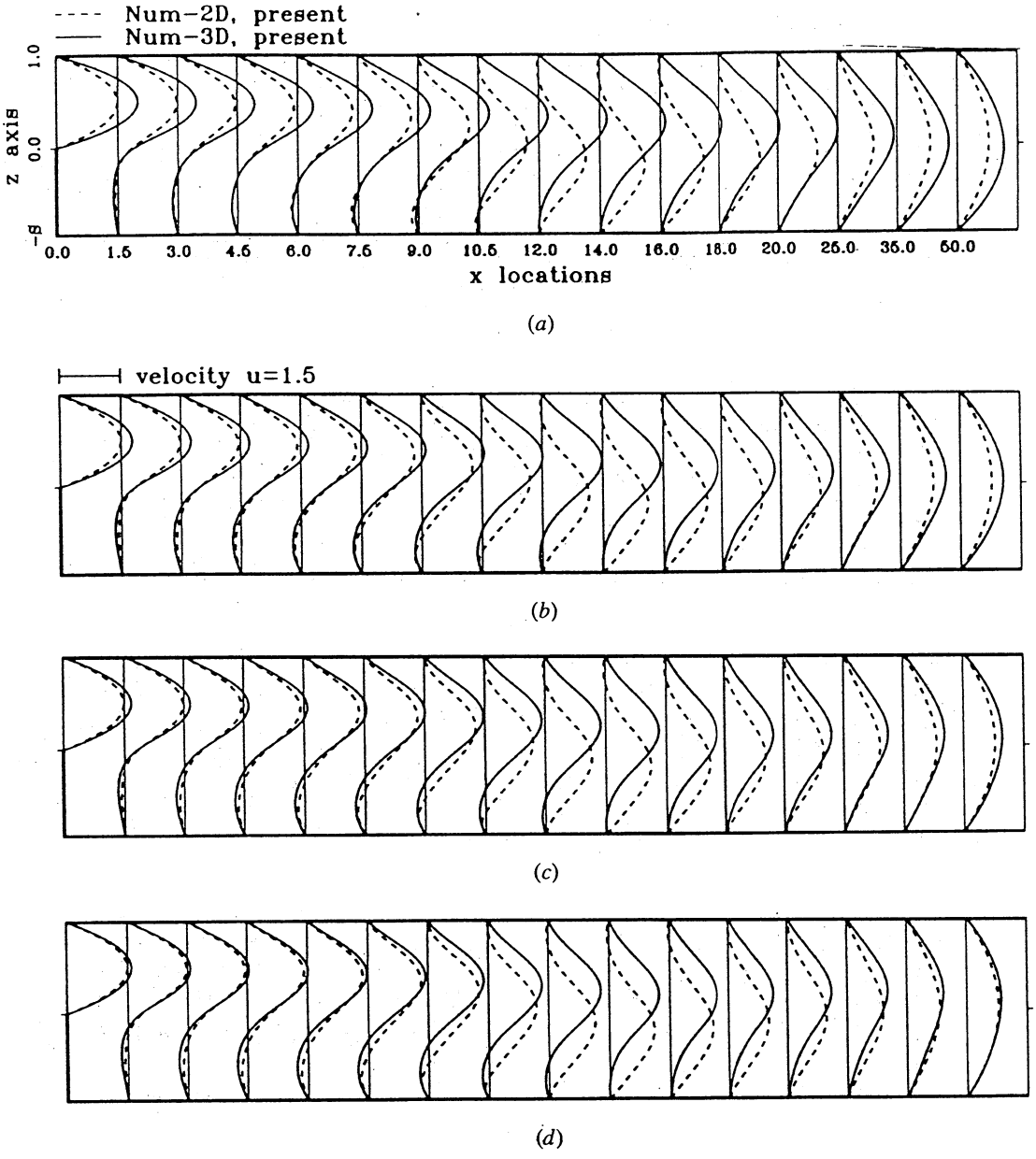

Figure 15. Comparison of 3-D (solid lines) and 2-D (dotted lines) velocity profiles at the symmetry plane for the case of Re = 800: (*a*) $B = 2$, (*b*) $B = 4$, (*c*) $B = 6$, and (*d*) $B = 10$.

study based on Re with values not greater than 800, and spans with the maximum value as high as 10.

Two conclusions can be drawn from this parametric study. For the Re investigated, the flow behavior tends to be 2-D with an increase of the span of the channel. Second, a 3-D flow structure is manifested by a spanwise spiraling flow behind the step. Notable is that particles spiral toward the symmetry plane with an increasingly large radius. Particles of this kind are located only near the two end walls.

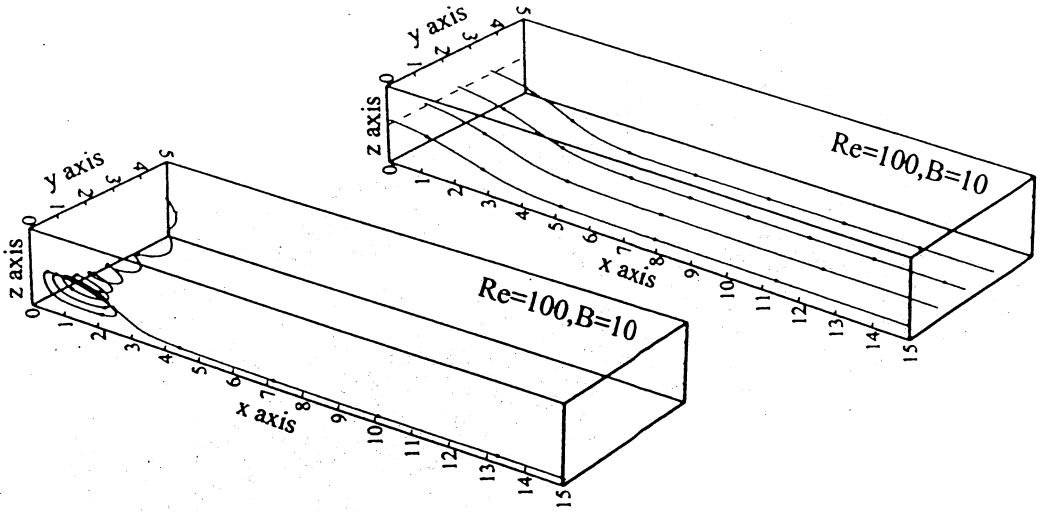

(*a*)

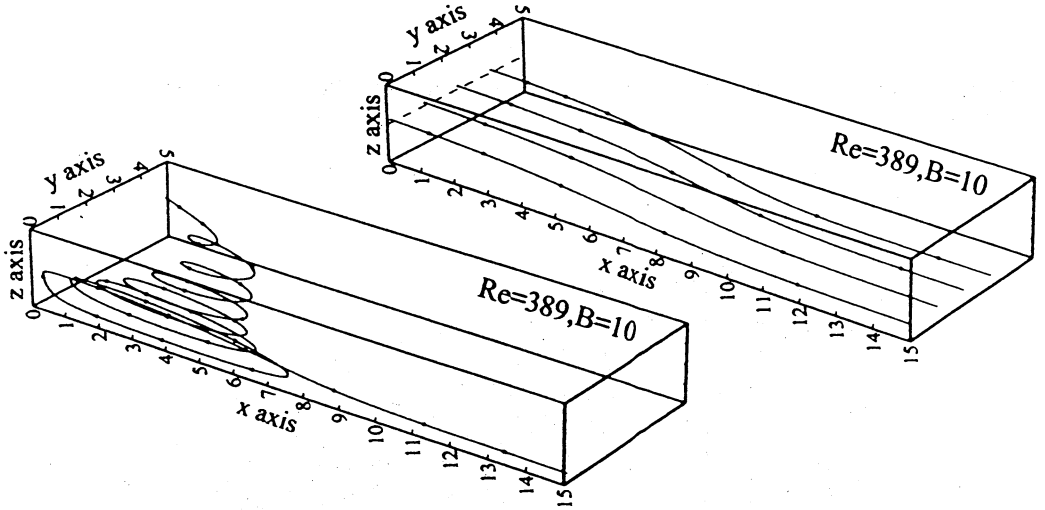

(*b*)

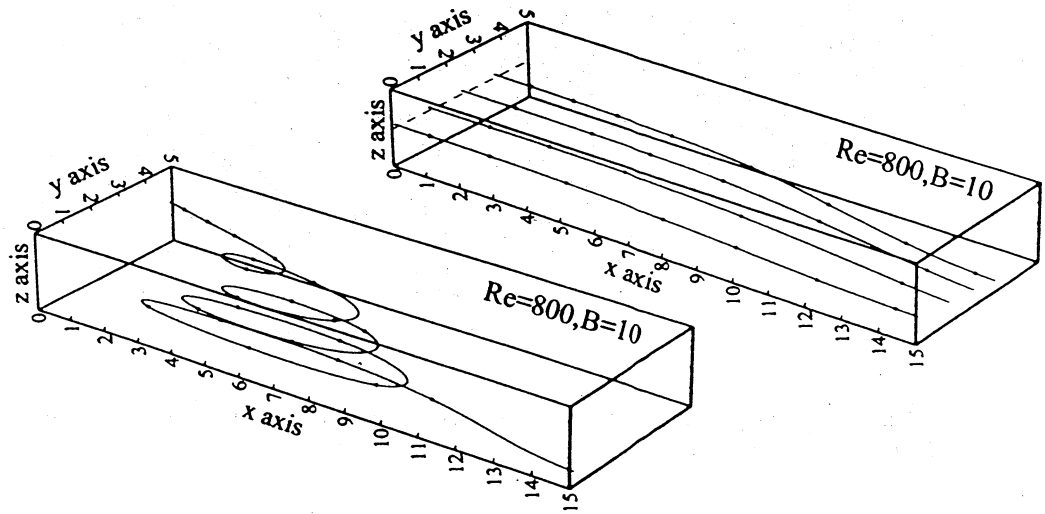

(*c*)

Figure 16. Illustration of 3-D spiralling/nonspiralling particle tracks for the case of $B = 10$. (*a*) Re = 100, (*b*) Re = 389, and (*c*) Re = 800.

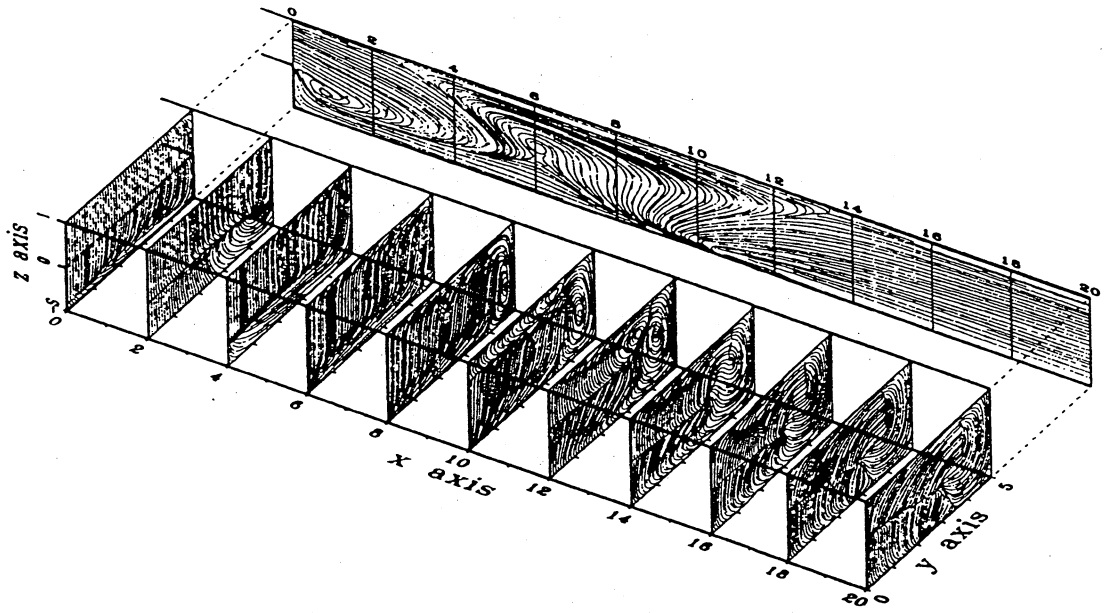

Figure 17. Evolution of streamlines on the transverse plane for the case of Re = 389 and B = 10.

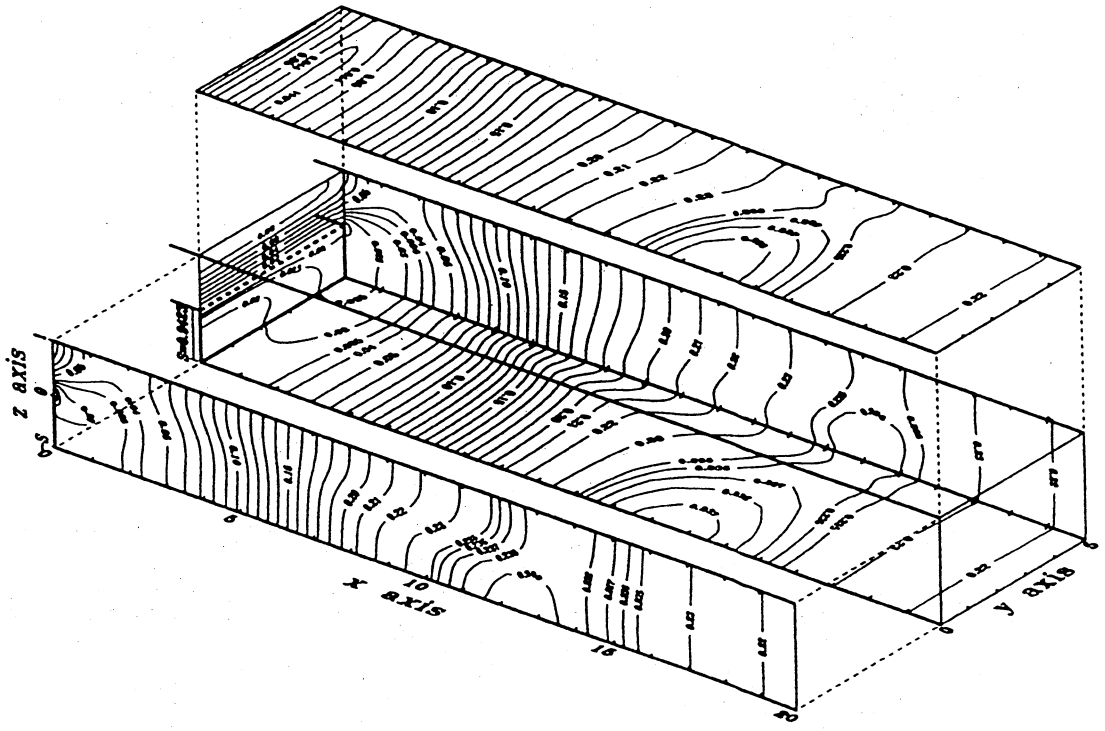

Figure 18. Computed pressure contours on the symmetry plane, roof, floor, step plane, and end wall for the case of Re = 389 and B = 10.

REFERENCES

1. K. Morgan, J. Periaux, and F. Thomasset (eds.), Analysis of Laminar Flow over a Backward-Facing Step, *A GAMM-Workshop*, Friedr Viewey & Sohn, Germany, 1984.
2. B. F. Armaly, F. Durst, J. C. F. Pereira, and B. Schönung, Experimental and Theoretical Investigation of Backward-Facing Step Flow, *J. Fluid Mech.*, vol. 127, pp. 473–496, 1983.
3. R. J. Goldstein, V. L. Eriksen, R. M. Olson, and E. R. G. Eckert, Laminar Separation Reattachment, and Transition of Flow over a Downward-Facing Step, *Trans. ASME D: J. Basic Eng.*, vol. 92, pp. 732–741, 1970.
4. C. Shih and C.-M. Ho, Three-dimensional Recirculation Flow in a Backward Facing Step, *ASME J. Fluids Eng.*, vol. 116, pp. 228–232, 1994.
5. J. Y. Yoo and S. J. Baik, Redeveloping Turbulent Boundary Layer in the Backward-Facing Step Flow, *ASME J. Fluids Eng.*, vol. 114, pp. 522–529, 1992.
6. G. Papadopoulos and M. V. Ötiigen, Separating and Reattaching Flow Structure in a Suddenly Expanding Rectangular Duct, *J. Fluids Eng.*, vol. 117, pp. 17–23, 1995.
7. M. V. Ötiigen, Expansion Ratio Effects on the Separated Shear Layer and Reattachment Downstream of a Backward-Facing Step, *Exp. Fluids*, vol. 10, pp. 273–280, 1991.
8. J. C. Vogel and J. K. Eaton, Heat Transfer and Fluid Mechanics Measurements in the Turbulent Reattaching Flow Behind a Backward-Facing Step, Technical Report MD-44, Department of Mechanical Engineering, Stanford University, Stanford, California, 1984.
9. L. Kaiktsis, G. E. M. Karniadakis, and S. A. Orszag, Onset of Three-Dimensionality, Equilibria, and Early Transition in Flow over a Backward-Facing Step, *J. Fluid Mech.*, vol. 231, pp. 501–528, 1991.
10. J. Kim and P. Moin, Applications of a Fractional-Step Method to Incompressible Navier-Stokes Equations, *J. Comput. Phys.*, vol. 59, pp. 308–323, 1985.
11. D. Kwak and J. L. C. Chang, A Three-dimensional Incompressible Navier-Stokes Flow Solver, Part 1: 2NS3D code, paper presented at the CFD workshop, University of Tennessee Space Institute, Tullahoma, 1985.
12. I. E. Barton, A Numerical Study of Flow over a Confined Backward-Facing Step, *Int. J. Numer. Methods Fluids*, vol. 21, pp. 653–665, 1995.
13. P. T. Williams and A. J. Baker, Incompressible Computational Fluids Dynamics and the Continuity Constraint Method for the Three-Dimensional Navier-Stokes Equations, *Numer. Heat Transfer Part B*, vol. 29, pp. 137–273, 1996.
14. T. Ikohagi, B. R. Shin, and H. Daiguji, Application of an Implicit Time-Marching Scheme to a Three-Dimensional Incompressible Flow Problem in Curvilinear Coordinate Systems, *Comput. Fluids*, vol. 21, no. 2, pp. 163–175, 1992.
15. P. T. Williams and A. J. Baker, Numerical Simulations of Laminar Flow over a 3D Backward-Facing Step, submitted to *Int. J. Numer. Methods Fluids*, 1995.
16. B. Jiang, L. Hou, and T. Lin, Least Squares Finite Element Solutions for Three-Dimensional Backward-Facing Step Flow, NASA-TM 106353, 1993.
17. F. M. White, *Viscous Fluid Flow*, 2nd ed., pp. 119–122, McGraw-Hill, New York, 1991.
18. F. H. Harlow and J. E. Welch, Numerical Calculation of Time-Dependent Viscous Incompressible Flow of Fluid with Free Surface, *Phys. Fluids*, vol. 8, pp. 2182–2189, 1965.
19. C. M. Rhie and W. L. Chow, A Numerical Study of the Turbulent Flow Past an Airfoil with Trailing Edge Separation, Report AIAA-82-0988, 1982.
20. J. C. Strikwerda, Finite Difference Methods for the Stokes and Navier-Stokes Equations, *SIAM J. Sci. Statist. Comput.*, vol. 5, pp. 56–68, 1984.
21. G. Schneider and M. Raw, Control Volume Finite Element Method for Heat Transfer and Fluid Flow Using Colocated Variables, 1: Computational Procedure, *Numer. Heat Transfer*, vol. 11, pp. 363–390, 1987.

22. S. Abdallah, Numerical Solutions of the Pressure Poisson Equation with Neumann Boundary Conditions Using a Nonstaggered Grid, *J. Comput. Phys.*, vol. 70, pp. 182–192, 1987.
23. S. V. Patankar, *Numerical Heat Transfer and Fluid Flow*, Hemisphere, Washington, D.C., 1980.
24. B. P. Leonard, A Stable and Accurate Convective Modeling Procedure Based on Quadratic Upstream Interpolation, *Comput. Methods Appl. Mech. Eng.*, vol. 19, pp. 59–98, 1979.
25. C. R. Ethier and D. A. Steinman, Exact Fully 3D Navier-Stokes Solutions for Benchmarking, *Int. J. Numer. Methods Fluids*, vol. 19, pp. 369–375, 1994.
26. T. P. Chiang, R. R. Hwang, and W. H. Sheu, Finite Volume Analysis of Spiral Motion in a Rectangular Lid-Driven Cavity, *Int. J. Numer. Methods Fluids*, vol. 23, pp. 325–346, 1996.
27. T. P. Chiang, W. H. Sheu, and R. R. Hwang, Three-Dimensional Vortex Dynamics in a Shear-Driven Rectangular Cavity, *Int. J. Comput. Fluid Dyn.*, in press, 1996.
28. L. A. Yates and G. T. Chapman, Streamlines Vorticity Lines, and Vortices Around Three-Dimensional Bodies, *AIAA J.*, vol. 30, no. 7, pp. 1819–1826, 1992.
29. R. Legendre, Séparation de Courant l'Écoulement Laminaire Tridimensionnel, *Rech. Aéro*, vol. 54, pp. 3–8, 1956.
30. M. Lighthill, Attachment and Separation in Three-Dimensional Flow, in L. Rosenhead II, (eds.), *Laminar Boundary Layers*, vol. 2.6, pp. 72–82, Oxford University, Press, 1963.
31. Y. Levy, D. Degani, and A. Seginer, Graphical Visualization of Vortical Flows by Means of Helicity, *AIAA J.*, vol. 28, no. 8, pp. 1347–1352, 1990.
32. M. M. T. Wang and T. W. H. Sheu, Implementation of a Free Boundary Condition to Navier-Stokes Equations, *Int. J. Numer. Methods Heat Fluid Flow*, in press, 1996.
33. A. G. Tomboulides, M. Israle, and G. E. Karniadakis, Viscous Sponge Outflow Boundary Conditions for Simulations of Incompressible Flows, paper presented at the Minisymp. on Outflow Boundary Conditions, Stanford, California, 1991.